J Mater Sci: Mater Electron
DOI 10.1007/s10854-016-6079-8

Preparation and characterization of CdZnTe multilayer films by repeated RF magnetron sputtering

Xiuying Gao[1,2] · Xinghua Zhu[1] · Hui Sun[1] · Dingyu Yang[1] · Peihua Wangyang[1] · Shifu Zhu[2]

Received: 6 August 2016 / Accepted: 12 November 2016
© Springer Science+Business Media New York 2016

Abstract $Cd_{1-x}Zn_xTe$ (CZT) multilayer films were repeatedly deposited by using RF magnetron sputtering with a $Cd_{0.9}Zn_{0.1}Te$ crystal target. The morphological, structural and optical properties of the CZT multilayer films were characterized. The thickness of the CZT films increases from 1360 to 9230 nm with the increase of the repeated deposition cycles. It is found that the mismatching of the thermal stress between the film and substrate was eliminated by repeated deposition, resulting in an improved adhesion and crystalline quality, larger grain size and decreased microvoids. X-ray diffraction patterns show that the polycrystalline structure CZT films with (111) plane preferred orientation was obtained. The band gap of the CZT films decreases from 1.517 to 1.500 eV resulting from Zinc loss during the repeated deposition and anneal. The density of the disordered state was decreased with the increasing of deposition layers.

1 Introduction

$Cd_{1-x}Zn_xTe$ (CZT) is one of the promising semiconductor materials for radiation detection, capable of operating at room temperature due to its large and tunable band gap (1.45–2.26 eV) and very low leakage current [1–3]. CZT films have been deposited by several preparation techniques, such as thermal evaporation, close-spaced sublimation and radio frequency (RF) magnetron sputtering [4–9]. Among the techniques utilized for preparation of CZT films, RF magnetron sputtering is an optional technique which having the advantages of good reproducibility, high-efficiency material utilization and high deposition rate [10]. Various process parameters including sputtering power, deposition temperature and annealing temperature were regulated to prepare CZT films with $Cd_{0.9}Zn_{0.1}Te$ crystals target [10–13]. In the area of radiation detection the thickness of CZT film usually is acquired above 250 μm to achieve sufficient absorption to X- and γ-ray photons [14]. The conventional magnetron sputtering method is difficult to meet the requirements of the thickness. Moreover, there is a serious thermal stress between CZT films and glass substrates, resulting in the CZT film locally thermal shrinkage and generating of microvoids.

In this paper, we report a method of repeated deposition of the CZT thick films on an indium tin oxide (ITO) substrate by using RF magnetron sputtering with a $Cd_{0.9}Zn_{0.1}Te$ crystals target. The CZT films were thickened by increasing of the repeated deposition cycles. And the mismatching of the thermal stress between the CZT film and substrate was eliminated by this means, resulting in an improved adhesion and crystalline quality, larger grain size and decreased microvoids.

2 Experimental

The CZT films were repeatedly deposited by using RF magnetron sputtering with a $Cd_{0.9}Zn_{0.1}Te$ (99.99%) target. The ITO coated glass substrate (Corning 7059) was cleaned by acetone and ethanol with ultrasonic vibration, washed repeatedly with deionized water, and finally dried by high-

✉ Xinghua Zhu
zxh@cuit.edu.cn

[1] Information Materials and Devices Application Key Laboratory of Sichuan Provincial Universities, Chengdu University of Information Technology, Chengdu, China

[2] Department of Materials Science, Sichuan University, Chengdu, China

Published online: 05 December 2016

www.spm.com.cn

purity argon (99.99%) gas flow. The substrate was placed parallel to the target with a vertical distance of 4 cm. Considering the tolerable temperature of ITO and melting point of elemental Cadmium, the substrate temperature was maintained at 300 °C. The sputtering power was 60 W. The base pressure before sputtering was 1.0 × 10^{-3} Pa. High purity Ar (99.99%) gas was used in sputtering process to eliminate formation of impurity phases that may occurred by presences of other gases like oxygen, and the sputtering gas pressure was set to be 5.0 Pa with a deposition time of 3 h for each deposition cycle. In the course the sample was thermal annealed in a N_2 atmosphere for 3 h at 400 °C. Using a repeated sputtering method, another four layers CZT films were prepared using the same process parameter. Meanwhile, the ladder-like (visual inspection) film was prepared with a molybdenum sheet mask for the convenience of observation and analysis, the masked parts will not be covered by the next layer film and shown up (shown in Fig. 1).

The morphology of each layer CZT film was investigated by using an optical microscope and a CSPM5000 atomic force microscope (AFM, contact mode) with CSPM image process software. The cross section image of the five layers CZT films was characterized by scanning electron microscope (SEM). The thickness of the each layer CZT film was measured by using a KLA-Tencor profiler with 1360 (1st layer), 1911 (2nd layer), 1963 (3rd layer), 1987 (4th layer), 2009 nm (5th layer), respectively. The total thickness of the five layers CZT film is 9230 nm. The elemental content analysis of each layer CZT film was carried out by energy dispersive spectrometer (EDS). X-ray diffraction (XRD) was performed using a DX-2500 CuKα radiation (1.54 Å, 30 kV, 20 mA) to obtain the structure of each layer CZT film. The scanning angle was varied from 20° to 80° with steps of 0.04°. The optical transmittance spectrum of the CZT films deposited in different deposition cycles as a function of wavelength was measured using a SHIMADZU UV2550 UV–Vis spectrophotometer (300–900 nm).

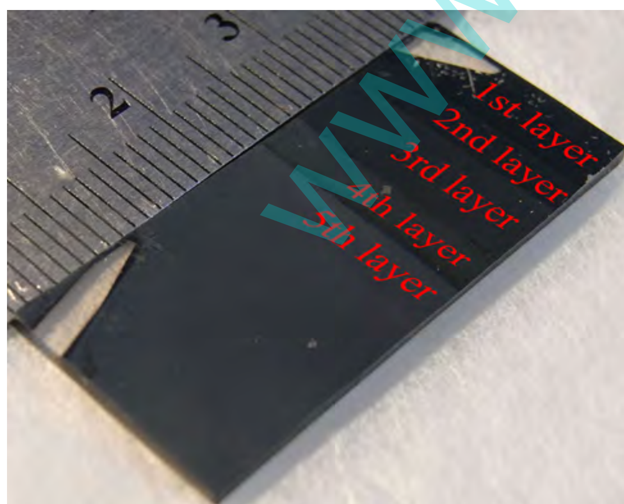

Fig. 1 Photograph of the five layers CZT films deposited in five deposition cycles

3 Results and discussion

3.1 Adhesion

Figure 2 shows the optical microscope images of the CZT films deposited by using RF magnetron sputtering in different deposition cycles. Figure 2a shows a large number of microviods in the first deposition cycle. The bright spots indicate the microviods of the CZT film. The growth of grain was inhibited due to the high deposition rate, which leads to small grain size and low adhesion, causing the appearance of microvoids. Meanwhile, the difference of thermal expansion coefficient between CZT films and ITO substrates leads to locally thermal shrinkage and mismatching of thermal stress, also causing the appearance of microvoids. Figure 2b–e indicates that the microviods gradually reduced to the fifth cycle completely disappeared with the increasing of deposition layers. By using the repeated deposition cycles, firstly, these microvoids will be filled when the crystals grain grew on the basis of the previous crystals. Secondly, the second layer grew again on the first layer which as the seed crystal layer and substrat, the thermal stress buffered on account of the same thermal expansion coefficient between the two layers. The front of the layer as a thermal stress buffer layer, with the increasing of deposition layer, the thermal stress gradually matches. Therefore, microvoids gradually decreased until disappear. These reasons resulted in the increase of grain size and adhesion, gradually decreased microvoids.

3.2 Morphology and structure

Figure 3a–e shows the surface morphology of each layer CZT film by repeatedly deposited cycles with the same deposition condition. Figure 3a shows the image of the first layer CZT film deposited on ITO coated glass substrate. The disordered film structure is constituted of irregular shape grain or microcrystal with a mean grain size of 100–115 nm. It indicates a poor crystalline degree, which can be attributed to the high deposition rate [12]. And the film shows small surface roughness and denser structure. The absence of microvoids is due to a small-scale scanning area 2 × 2 μm which smaller than the size of microvoids and no microvoid by coincidence in this scanning area. Figure 3b shows the surface morphology of the second layer CZT film deposited on the first layer. The mean grain

www.spm.com.cn

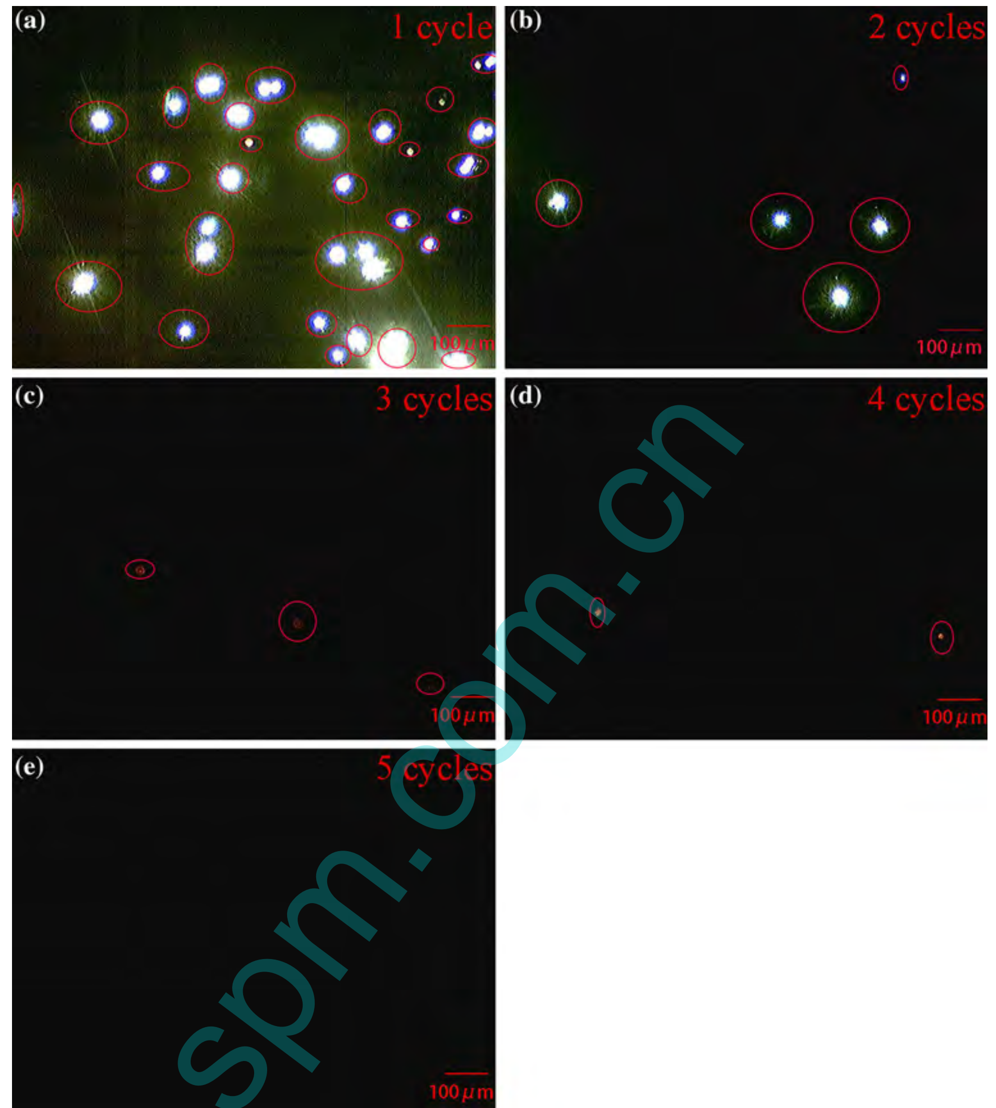

Fig. 2 Optical microscope image for the CZT films in different deposited cycles

www.spm.com.cn

size is 135–145 nm accompanying considerable grain boundary appearing compared with the first layer. It is thought that the second layer continuously grow on the first layer which as a seed crystal layer. Meanwhile, lots of small grains are observed on the second layer on account of the new crystal nucleus spontaneously forming during the second deposition. Compared with the first two layers, the third layer has more regular shape grain and larger grain size of 160–170 nm, as shown in Fig. 3c. Figure 3d, e shows a more complete grain shape, denser structure and better crystalline degree in regard to the fourth and fifth layer. The mean grain size of the fifth layer is about 253 nm, which is two times of the first layer's, which indicates that the grain size increasing with repeated deposition. The root-mean-square (RMS) roughness of the five layers CZT films can be obtained from the CSPM image software analysis. The linear variation of the mean grain size and roughness as a function of the number of the deposition layers is shown in Fig. 3f. These results indicate that the roughness of the film is increased resulting from the enlarging grain size with repeated deposition, corresponding to the analysis of optical microscope.

Figure 4 shows the cross-section SEM image of the five layers CZT films. It should be noted that there is no obvious interfaces between CZT layers, which indicates that the stress originated from the mismatch of lattice constant and thermal expansion coefficient was gradually buffered. On the other hand, the grains grown also results in low defects and stress with the increasing of thermal annealed times. This result is consistent with the analysis obtained from the optical microscope.

Figure 5a presents XRD spectra of five layers CZT films obtained by using repeated RF magnetron sputtering deposition. Five layers show the polycrystalline structure and (111) plane preferred orientation. The diffraction peaks appeared at $2\theta = 23.84°$, 39.35°, and 46.60° are identified

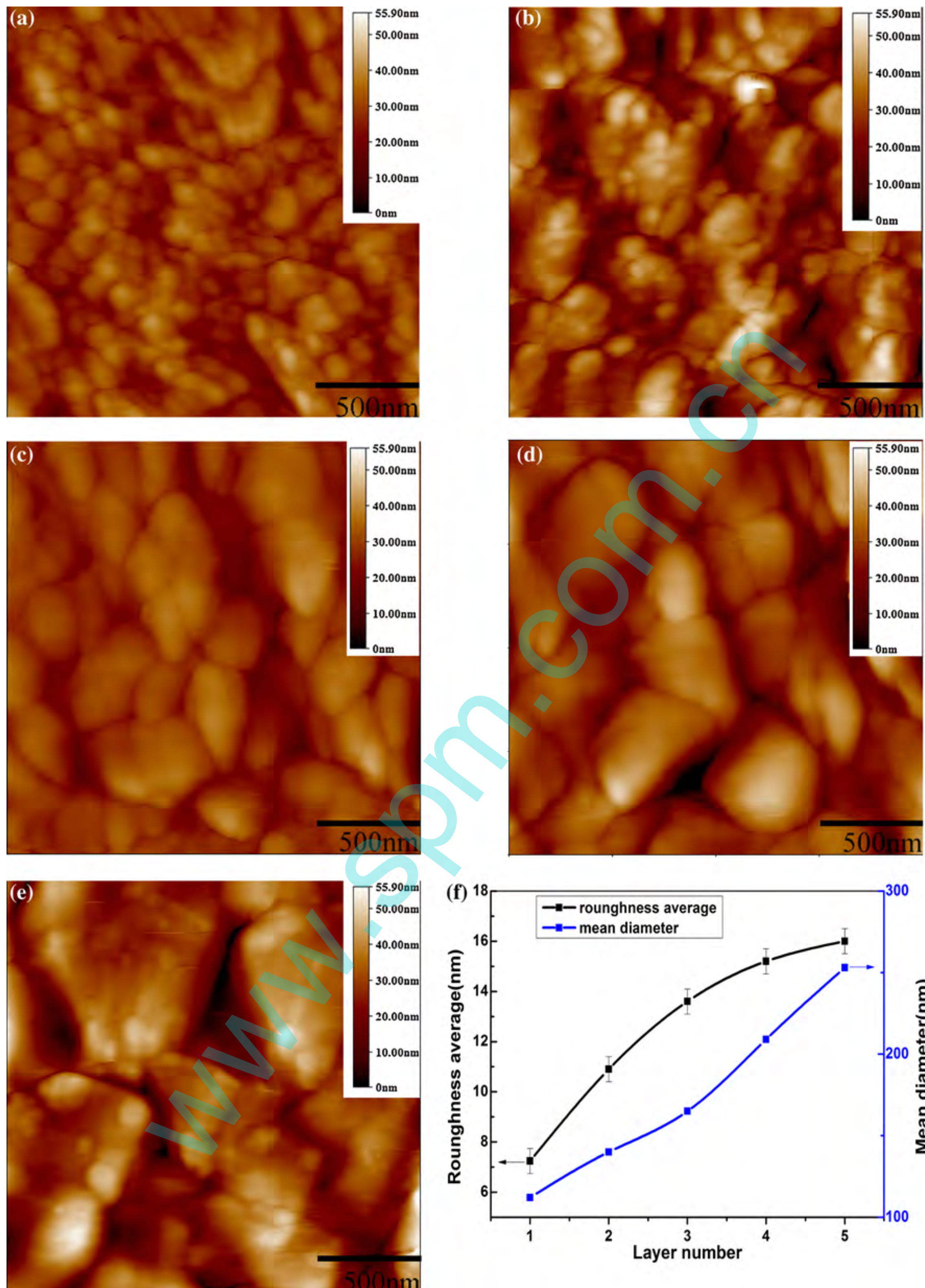

Fig. 3 The AFM micrographs of the CZT film **a** the first layer, **b** the second layer, **c** the third layer, **d** the forth layer and **e** the fifth layer, **f** the roughness average of the five layers CZT films obtained from AFM micrographs

www.spm.com.cn

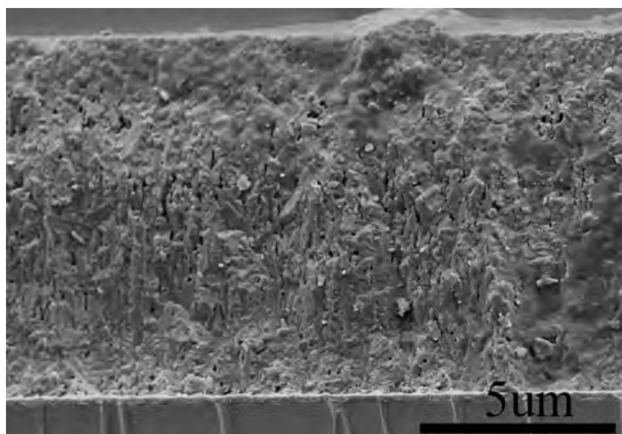

Fig. 4 Cross-section SEM images of the five layers CZT films deposited in five deposition cycles

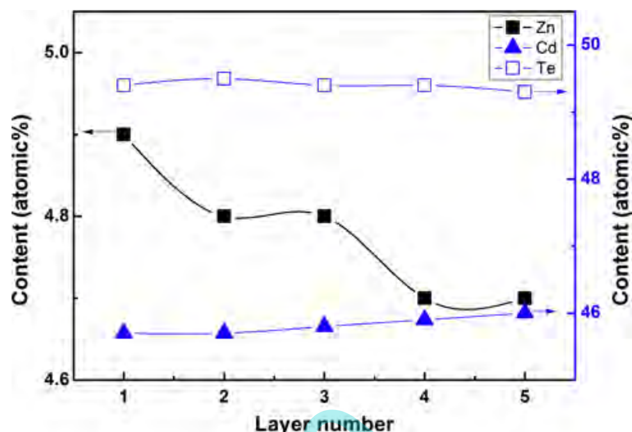

Fig. 6 Chemical elements contents of the CZT film for various deposition layers

as the (111), (220) and (311) plane, respectively. The intensity of (111) plane strengthen with the repeated deposition, indicating the better crystalline degree in agreement with the results from AFM analysis. The full width at half maximum (FWHM) value of (111) plane versus various deposition layers is plotted in Fig. 5b. The FWHM of (111) plane decreases with the repeated deposition, resulting from a preferable crystalline degree. The characterization of morphology and structure shows that repeated deposition is an effective method to obtain quality CZT thick films with increased grain, preferable crystalline degree and absence of microvoids.

3.3 Composition

The variation of chemical elements content (Cd, Zn and Te) of the five layers CZT films with various deposition cycles is shown in Fig. 6. The composition of each layer CZT film is not completely consistent with the $Cd_{0.9}Zn_{0.1}Te$ target, which is a common phenomenon in magnetron sputtering experiments [10, 11]. There is a small increase of Cd concentration and invariant of Te in the films with repeated deposition. However, the Zn concentration decreases with a loss rate of 2–6%. This behavior ascribes to the different energy transfer coefficient and sticking coefficient. In the sputtering process, the factor of energy transfer given by Winters and Sigmund [15],

$$\gamma = 4M_1 \cdot M_2/(M_1 + M_2)^2 \quad (1)$$

where M_1 is the quality of the incident ion (Ar^+) and M_2 is the quality of the target atom. We find that $\gamma_{Ar-Zn} = 0.94$, $\gamma_{Ar-Cd} = 0.78$ and $\gamma_{Ar-Te} = 0.73$. There was a difference in the energy transfer efficiency among the target atoms. The factor of energy transfer of Cd ($\gamma_{Ar-Cd} = 0.78$) under argon plasma is higher than Te ($\gamma_{Ar-Te} = 0.73$), causing Cd content in the films is higher than in target material. The factor of energy transfer of Zn is the highest, but Zn atom concentration in the crystal targets is very low, the energy transfer efficiency could be ignored. Meanwhile, Zn was

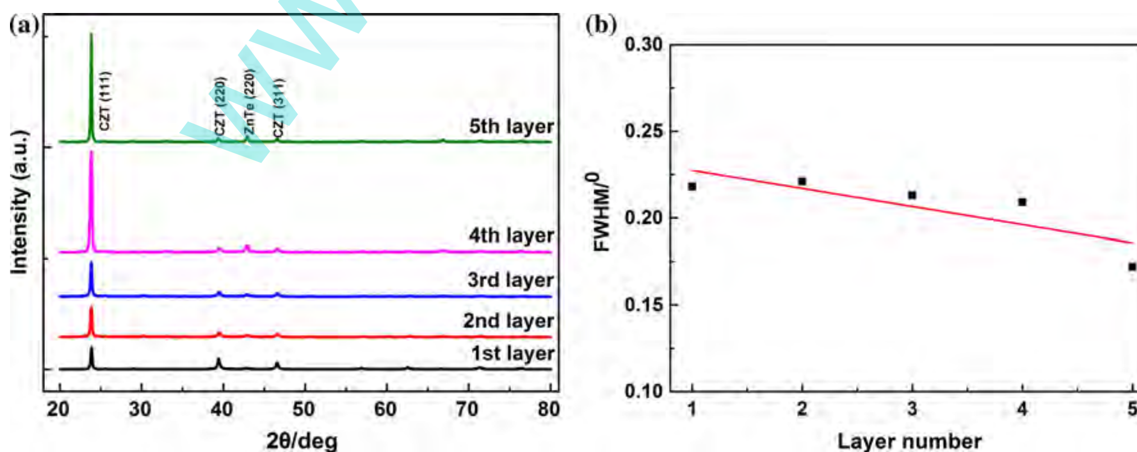

Fig. 5 **a** X-ray diffraction spectra of the five deposition layers, **b** variation of the FWHM of (111) peak as a function of the deposition layers

www.spm.com.cn

lost during the deposition and annealing due to the small sticking coefficient. These reasons led to the content of zinc is lower than the target material.

3.4 Band gap

The optical transmittance of the five CZT films in the wavelength range 300–900 nm were measured, as shown in Fig. 7a. The measured intensity I of transmitted light decreases with an increase of deposition layers which can be related to the film thickness. The transmittance data were used to calculate absorption coefficients of the CZT film in different deposition cycles. The absorption coefficient α is given by [16]:

$$I = I_0 \exp(-\alpha d) \quad (2)$$

where I is the intensity of transmitted light, I_0 is the intensity of incident light and d is the thickness of the CZT film. For a direct band gap semiconductor, the photon energy hν dependence of the absorption coefficient α can be described by the quadratic relation [6]:

$$(\alpha h\nu)^2 = \mathrm{A}\left(\mathrm{h}\nu - E_g\right) \quad (3)$$

where A is a constant and E_g is the optical band gap of the film.

The E_g value was obtained from the intercept on hν axis $(\alpha \mathrm{h}\nu)^2 = 0$, as shown in Fig. 7b. The value of E_g decreases from 1.517 to 1.500 eV with the increase of deposition layers. Due to the optical band gap of the CZT film is closely related to the stoichiometric proportion, in order to analyze the relationship between them, a fitting curve is obtained by the data of the optical band gap and the Zn content, as shown in Fig. 7c. The equation is as follows,

$$E_g = 1.45 + 0.59x + 0.22x^2 \quad (4)$$

where E_g is the optical band gap of CZT, CdTe and ZnTe. The optical band gap values considered for CdTe and ZnTe were 1.45 and 2.26 eV [17, 18], respectively. The result is compatible with the theoretical calculation [19]. It indicates the repeatedly deposition and annealing processes led to the loss of Zn, which diminished the optical band gap.

The optical band gap is also related to the microstructure of CZT film. The absorption presents an apparent trailing phenomenon which is the so-called Urbach tail [20]. Generally, it is thought that the Urbach tail generated from the disordered structure, and its width (E_0) is related to the

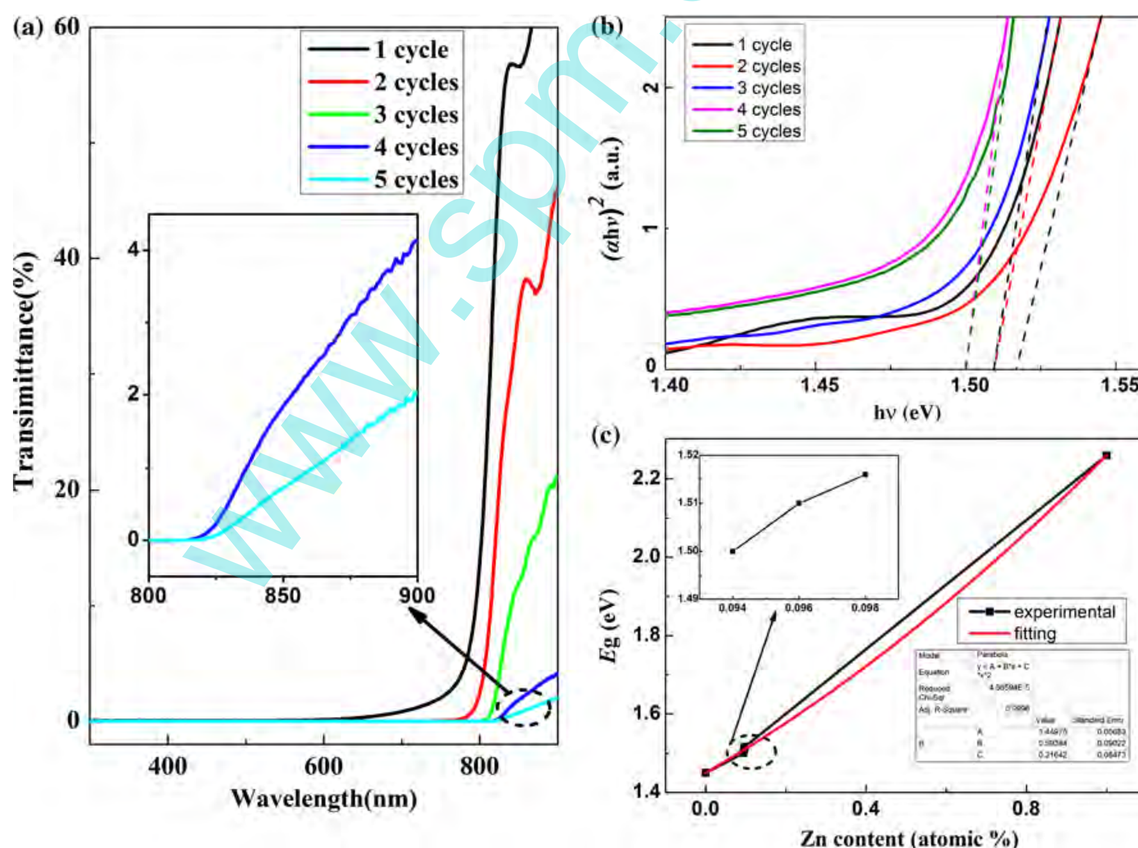

www.spm.com.cn

Fig. 7 **a** Transmission spectra of the five CZT films deposited in different deposition cycles. **b** $(\alpha h\nu)^2$ versus hν to determine the optical band gap of the five CZT films. **c** The relationship between Zn content and the optical band gap

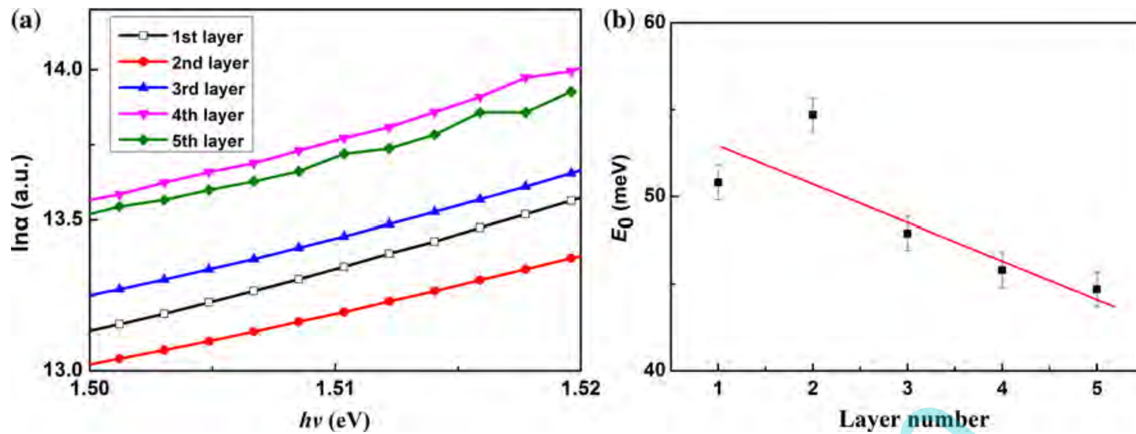

Fig. 8 **a** Linear plot of ln α versus photon energy hν. **b** Urbach tail width of the CZT films versus the five deposition layers

density of the disordered state. The value of E_0 is determined by the Urbach formula [21],

$$\alpha = \alpha_0 \exp\left[\left(h\nu - E_g\right)/E_0\right] \quad (5)$$

where α_0 is the Urbach absorption at the edge (E_g). The relationship ln α against hν is shown in Fig. 8a, where a linear relationship is observed. E_0 can be obtained by taking the inverse of the slope (1/slope) from the linear part of the curve. The plotting of Urbach tail width versus deposition layers is shown in Fig. 8b, the value of E_0 decreases with the increasing of the deposition layers. It demonstrates that the density of the disordered state was decreased with the increasing of the deposition layers. This result is agree with the analysis results obtained from XRD.

4 Conclusion

The multilayer CZT films were prepared by repeatedly RF magnetron sputtering with a $Cd_{0.9}Zn_{0.1}Te$ target and same process parameters. As the deposition layers increases, the thickness of the CZT films was increased from 1360 to 9230 nm, the crystal grain gradually grew resulting in larger grain size, and the mean grain size increase from 115 to 253 nm. During the repeated deposition cycles, the mismatching of the thermal stress between the film and substrate was gradually eliminated which lead to an improved adhesion and crystalline degree, absence of microvoids. The five layers CZT films showed the zinc blend structure with predominant (111) orientation. With the increasing of deposition layers, Zn was lost during the repeatedly depositing and annealing and the density of the disordered state was decrease, which resulting in the optical band gap of the five CZT films decreases from 1.517 to 1.500 eV. One can see that the value of band gap has no remarkable variation which indicates the repeated deposition method has no significantly effect. These experiment results show that repeated RF magnetron sputtering is effective to deposit thicker film with excellent properties.

Acknowledgements This work was supported by the Scientific Research Fund of Sichuan Provincial Education Department No.15ZB0173, 2016Z037, the Support Program Fund of Science and Technology of Sichuan Province No. 2014GZ0020, 2015GZ0194, No. 2014GZX0012 and 2016FZ0018, and the National Natural Science Foundation of China Grant No. 11675029.

www.spm.com.cn

References

1. K. Mochizuki, J. Takahashi, N. Nakamura, Phys. Status Solidi C **6**, 528–531 (2015). doi:10.1002/pssc.201400264
2. S. Tokuda, H. Kishihara, S. Adachi, T. Sato, J. Mater. Sci.: Mater. Electron. **15**, 1–8 (2004). doi:10.1023/A:1026297416093
3. R.M. Krishna, S.K. Chaudhuri, K.J. Zavalla, K.C. Mandal, Nucl. Instrum. Methods Phys. Res. A **701**, 208–213 (2013). doi:10.1016/j.nima.2012.10.131
4. K.H. Kirn, Y.H. Na, Y.J. Park, T.R. Jung, Nucl. Sci. Symp. Conf. Rec. **5**, 4308 (2003). doi:10.1109/NSSMIC.2003.1352636
5. X. Haitao, X. Run, J. Huang, J. Zhang, K. Tang, L. Wang, Appl. Surf. Sci. **305**, 477 (2014). doi:10.1016/j.apsusc.2014.03.117
6. H. Zhou, D. Zeng, S. Pan, Nucl. Instrum. Methods Physi. Res. Sect. A: Accel. Spectrom. Detect. Assoc. Equip. **698**, 81 (2013). doi:10.1016/j.nima.2012.09.024
7. J. Huang, L.J. Wang, K. Tang, R. Xu, J.J. Zhang, Y.B. Xia, X.G. Lu, Phys. Procedia **32**, 161 (2012). doi:10.1016/j.phpro.2012.03.535
8. D.M. Zeng, W.Q. Jie, H. Zhou, Y.G. Yang, F. Chen, Adv. Eng. Mater. **2312**, 194–196 (2011). doi:10.4028/www.scientific.net/AMR.194-196.2312
9. E. Yilmaz, E. Tugay, A. Aktag, I. Yildiz, M. Parlak, R. Turan, J. Alloys Compd. **545**, 90 (2012). doi:10.1016/j.jallcom.2012.08.028
10. D. Zeng, W. Jie, H. Zhou, Y. Yang, Thin Solid Films **519**, 4158–4161 (2011). doi:10.1016/j.tsf.2011.01.378
11. H. Malkaş, S. Kaya, E. Yılmaz, J. Electron. Mater. **43**, 4011–4017 (2014). doi:10.1007/s11664-014-3371-3
12. E. Yılmaz, Energy Sources A **34**, 332–335 (2012). doi:10.1080/15567036.2010.490824

13. A.S. Pugalenthi, R. Balasundaraprabhu, S. Prasanna, K. Thilagavathy, N. Muthukumarasamy, S. Jayakumar, Mater. Technol. **30**, 200–204 (2015). doi:10.1179/1753555714Y.0000000244
14. S. Kasap, J.B. Frey, G. Belev, O. Tousignant, H. Mani et al., Sensors **11**, 5112–5157 (2011). doi:10.3390/s110505112
15. H.F. Winters, P. Sigmund, J. Appl. Phys. **45**, 4760 (1974). doi:10.1063/1.1663131
16. R. Swanepoel, J. Appl. Phys. **45**, 4760–4767 (1974). doi:10.1088/0022-3735/16/12/023
17. J.E. Toney, T.E. Schlesinger, R.B. James, Nucl. Instrum. Methods **A428**, 14–24 (1999). doi:10.1016/S0168-9002(98)01575-7
18. K. Prasada Rao, O.M. Hussain, K.T.R. Reddy, P.S. Reddy, S. Uthanna, B.S. Naidu, P.J. Reddy, Opt. Mater. **5**(1–2), 63–68 (1996). doi:10.1016/0925-3467(95)00041-0
19. O. Zelaya-Angel, J.G. Mendoza-Alvarez, M. Becerril, H. Navarro-Contreras, L. Tirdo-Mejia, J. Appl. Phys. **95**, 6284–6288 (2004). doi:10.1063/1699493
20. F. Urbach, Phys. Rev. **92**, 1324 (1953). doi:10.1103/PhysRev.92.1324
21. J.I. Pankove, Phys. Rev. A **140**, 2059 (1965). doi:10.1103/PhysRev.140.A2059

www.spm.com.cn